The Astrophysical Journal Letters, 861:L26 (5pp), 2018 July 10 https://doi.org/10.3847/2041-8213/aacf40

Discovery of a 3 s Spinning Neutron Star in a 4.15 hr Orbit in the Brightest Hard X-Ray Source in M31

Guillermo A. Rodríguez Castillo[1], Gian Luca Israel[1], Paolo Esposito[2], Alessandro Papitto[1], Luigi Stella[1], Andrea Tiengo[3,4,5], Andrea De Luca[4], and Martino Marelli[4]
[1] INAF—Osservatorio Astronomico di Roma, via Frascati 33, I-00078 Monteporzio Catone, Italy; guillermo.rodriguez@oa-roma.inaf.it, grodriguezcas@gmail.com
[2] Anton Pannekoek Institute for Astronomy, University of Amsterdam, Science Park 904, NL-1098 XH Amsterdam, The Netherlands
[3] Scuola Universitaria Superiore IUSS, piazza della Vittoria 15, I-27100 Pavia, Italy
[4] INAF—Istituto di Astrofisica Spaziale e Fisica Cosmica—Milano, via E. Bassini 15, I-20133 Milano, Italy
[5] INFN—Istituto Nazionale di Fisica Nucleare, Sezione di Pavia, via A. Bassi 6, I-27100 Pavia, Italy
Received 2018 April 28; revised 2018 June 15; accepted 2018 June 19; published 2018 July 13

Abstract

We report the discovery with *XMM-Newton* of 3 s X-ray pulsations from 3XMM J004232.1+411314, a dipping source that dominates the hard X-ray emission of M31. This finding unambiguously assesses the neutron star (NS) nature of the compact object. We also measured an orbital period of 4.15 hr and a projected semi-axis at $a_X \sin i = 0.6$ lt-s, which implies a low-mass companion of about 0.2–0.3 $M_\odot$ assuming an NS of 1.5 $M_\odot$ and an orbital inclination $i = 60°$–$80°$. The barycentric orbit-corrected pulse period decreased by ∼28 ms in about 16 year, corresponding to an average spin-up rate of $\dot{P} \sim -6 \times 10^{-11}$ s s^{-1}; pulse period variations, probably caused by X-ray luminosity changes, were observed on shorter timescales. We identify two possible extreme scenarios for the source: a mildly magnetic NS with $B_p \simeq$ few $\times 10^{10}$ G if the pulsar is far from its equilibrium period P_{eq} and the disk is truncated at the value of the Alfvén radius corresponding to the observed luminosity, and a relatively young, highly magnetic NS with $B_{eq} \simeq 2 \times 10^{13}$ G if spinning close to P_{eq} and the disk is truncated close to the co-rotation surface.

Key words: galaxies: individual (M31) – stars: neutron – X-rays: binaries – X-rays: individual (3XMM J004232.1+411314, CXOM31 J004232.0+411314, Swift J0042.6+4112)

1. Introduction

At a distance $d = 780$ kpc (Holland 1998), M31 is the closest major galaxy to the Milky Way. Despite a number of extensive studies, only one accreting X-ray neutron star (NS) pulsar binary has been securely identified so far, 3XMM J004301.4+413017 (spin and orbital periods of 1.2 s and 1.3 days, respectively; Esposito et al. 2016, but see also Zolotukhin et al. 2017). Here we report the discovery of pulsations from 3XMM J004232.1+411314 (3X J0042 hereafter), a luminous X-ray source located in the inner bulge of M31, about 3.7 arcmin from the center, which was detected in all of the X-ray surveys of M31 conducted with good-resolution imaging instruments (see Vulic et al. 2016, and references therein). Its luminosity was found to be consistently above 10^{37} erg s^{-1}. Based on its spectral shape, luminosity, and moderate variability, the source was suggested to be an X-ray binary. Using *NuSTAR* Yukita et al. (2017) pinpointed 3X J0042 as the soft X-ray counterpart of Swift J0042.6+4112, whose hard X-ray emission (≳20 keV) dominates the bulge of M31 (Baumgartner et al. 2013; Revnivtsev et al. 2014). After examining all available multi-wavelength information, Yukita et al. (2017) concluded that 3X J0042 could be either an X-ray pulsar with an intermediate-mass companion (stellar counterparts heavier than 3 $M_\odot$ are disfavored by the *Hubble Space Telescope* (*HST*) images) or a symbiotic X-ray binary. During the analysis of the *XMM-Newton* X-ray data archive carried out within the Exploring the X-ray Transient and variable Sky (EXTraS) project,[6] Marelli et al. (2017) discovered dips recurring with a period of ∼4 hr in the light curve of 3X J0042, likely reflecting the orbital period of the system. This prompted them to propose that the source is a low-mass X-ray binary (LMXB) seen at high inclination (60°–80°, following Frank et al. (1987) for LXMB showing dips).

In this Letter, based on the detailed timing analysis of the whole *XMM-Newton* archival data of 3X J0042, we report on the discovery of 3 s pulsations in nine pointings over 16 years; furthermore, pulse arrival time delays unambiguously provide an orbital period of 4.15 hr, in agreement with the findings of Marelli et al. (2017). We discuss the nature of the source in the light of these results.[7]

2. Data Analysis and Results

The region of 3X J0042 was observed 48 times by *XMM-Newton* with the European Photon Imaging Camera (EPIC) pn and Metal Oxide Semi-conductor (MOS) cameras operating in different observational modes (the most relevant differences being the time resolution and size of the field of view; see Strüder et al. 2001; Turner et al. 2001). The raw observation data files were processed with the Science Analysis Software (SAS) v.16. Time intervals with high particle background were filtered out. Photon event lists were extracted from a 31 arcsec radius around the source, while the background was estimated

[6] See De Luca et al. (2016) and http://www.extras-fp7.eu.

[7] During the peer review process of this Letter, we became aware of a proceeding abstract by Yukita et al. (2018) mentioning a 3 s spin period candidate and a 6.1 days orbital period, based on *Nuclear Spectroscopic Telescope Array* (*NuSTAR*) data and on a recent long *XMM-Newton* observation of 3X J0042 (Obs.ID 0790830101, see Table 1). The abstract does not provide uncertainties in the period value (note, however, the much longer orbital period), thus we are unable to assess whether their candidate signal is compatible with our discovery.

Table 1
The *XMM-Newton* Observations in which the 3 s Spin Period was Detected

Data Set # Obs.ID	Date[a] (TJD)	Period (s)	PF[b] (%)	L_X[c] (erg s^{-1})
1. 0109270101	12089.6	3.00864(2)	11(2)	0.69(1)
2. 0112570101	12281.1	3.00816(1)	14(2)	0.69(1)
3. 0405320501	13918.7	3.00295(5)	14(2)	1.04(3)
4. 0650560301	15565.9	2.99627(2)	11(2)	1.02(2)
5. 0650560601	15596.1	2.99617(3)	14(2)	1.02(2)
6. 0674210301	15933.2	2.99457(8)	11(2)	1.14(3)
7. 0674210601	15957.2	2.99422(4)	11(2)	1.22(2)
8. 0764030301	17403.9	2.98443(3)	16(1)	1.90(6)
9. 0790830101	17774.6	2.981041(6)	14(1)	2.12(4)

Notes. Figures in parentheses represent the 1σ uncertainties in the least significant digit.
[a] Mid-point of the observation.
[b] Pulsed fraction, defined as the semi-amplitude of the sinusoid divided by the average source count rate.
[c] In units of 10^{38} and in the 0.2–12 keV band.

from a nearby circular region with the same radius, which excluded other sources and charge-coupled device (CCD) gaps. Our timing analysis was based on the pn data, as they offer the highest time resolution. Photon arrival times were converted to the barycentre of the Solar system with the SAS task BARYCEN.

The technique that we used to search the pn data for periodic signals is a generalization of the Fourier-based procedure outlined in Israel & Stella (1996), where we also included "de-acceleration" corrections for both the first period derivative and the Doppler delays. Each photon arrival time is corrected according to the expression: $t' = t - (a_X \sin i/c) \sin [2\pi(t - T_{node})/P_{orb}]$, where t is the photon arrival time, $a_X \sin i$ is the semi-axis projection on the orbital plane, c is the speed of light, P_{orb} is the orbital period, and T_{node} is the time of the ascendant node. This correction is applied for each combination of P_{orb}, $a_X \sin i$, and T_{node} in a three-dimension grid with given parameter steps. Then, the procedure is reiterated within a vector of $\dot{P}$ values. Because this approach is highly CPU-time-consuming, we adopted the orbital period of ∼4.01 hr inferred from the dips recurrence by Marelli et al. (2017) as our initial guess and also took into account the (reasonable) constraints on the maximum mass of the companion derived by Yukita et al. (2017).

The first run of the search over the observation with the longest exposure and the highest count rate (Obs.ID 0790830101, see Table 1) revealed a strong signal (12σ confidence level, c.l.) at approximately 2.98 s for the grid point [$P_{orb} = 14280$ s, $a_X \sin i = 0.54$ lt-s, $T_{node} = 17774.3$ truncated Julian day (TJD)]. We performed a phase-fitting analysis of the ∼4 orbital cycles covered by this observation (see Dall'Osso et al. 2003 for details), in order to measure more precisely the orbital parameters. The phase of the pulses was determined over 34 consecutive time intervals, as shown in Figure 2 (left panel). The best-fitting orbital parameters are reported in Table 2. These honed values were then fed as inputs to the search algorithm for the remaining 47 observations. We detected the ∼3 s signal at a c.l. higher than 3.5σ in eight more observations (see Table 1 and Figure 1; note that in obs.ID 0109270101 the signal was unambiguous, but just below the detection threshold). For each detection, the period estimate was refined with the phase-fitting analysis. Intrinsic (spin up or down of the pulsar) $\ddot{P}$ components were not detected within single observations, with a 3σ upper limit of about 3×10^{-9} s s^{-1} in the most stringent case.

Table 2
Orbital Parameters of 3X J0042

Parameter	Value
Orbital period, P_{orb} (hr)	4.15(4)
Epoch of ascending node, T_{node} (TJD)	17774.525(3)
Projected semi-axis, $a_X \sin i$ (lt-s)	0.59(4)
Mass function, $f(M)$ ($M_\odot$)	$7(2) \times 10^{-3}$
Companion mass[a] ($M_\odot$)	0.22–0.32

Notes. Numbers in parentheses represent 1σ uncertainties on the last significant digit.
[a] For i between 60° and 80°, as estimated by Marelli et al. (2017), and an NS with mass of 1.5 $M_\odot$. The range widens to 0.19–0.46 $M_\odot$ for NS masses in the (1–2.8) $M_\odot$ interval.

Figure 2 (right panel) shows the period evolution, whereas Figure 3 displays a collection of all light curves folded at the best-fit period of each data set (see also Table 1). No significant change of the pulsed fraction as a function of energy was detected, likely owing to the softness of the source and poor statistics at energies above ∼4 keV. From TJD 12089 (2001 June 29) to 17774 (2017 January 21), the average spin-up rate of 3X J0042 was $\dot{P} \sim -5 \times 10^{-11}$ s s^{-1}. However, the period evolution displays clear departures from a constant $\dot{P}$. Both the luminosity and spin evolution of the source (see the right panel of Figures 2 and 1 of Marelli et al. 2017) appear to have changed around TJD 16000, after which a substantial steepening of the spin-up rate took place and the luminosity approximately doubled. We estimate that the average $\dot{P}$ was $\sim -4.2 \times 10^{-11}$ and -8.5×10^{-11} s s^{-1} before and after TJD ∼16,000, respectively (note that the period measurements are too sparse to better constrain the epoch and the pace of the $\dot{P}$ change).

For all remaining data sets, we derived 3σ upper limits on the pulsed fraction over an interval of trial periods determined by using the $\dot{P}$ measurements. The average 3σ upper limit on the pulse fraction in the 39 observations is ∼26%, the most stringent limit being 18%. It is therefore possible that the flux modulation at 3 s is always present (the highest value measured, that of Obs.ID 0764030301, is 16%, cf. Table 1), but remained undetected in those data sets owing to poor statistics.

3. Discussion

The accretion disk around a magnetized NS is truncated at a radius that is usually estimated as a fraction ξ of the Alfvén radius

$$R_{in} = 68.7\, \xi_{0.5}\, M_{*,1.4}^{1/7}\, R_{*,10}^{-2/7} (\eta^{-1} L_{38})^{-2/7} \mu_{28}^{4/7} \text{ km}. \quad (1)$$

Here, $M_{*,1.4}$ and $R_{*,10}$ are the NS mass and radius in units of 1.4 $M_\odot$, and 10 km, respectively, L_{38} is the X-ray luminosity in units of 10^{38} erg s^{-1}, $\eta = L_X R_*/(GM\dot{M}) = 1$ is the accretion efficiency, μ_{28} is the magnetic dipole moment in units of 10^{28} G cm^2, and ξ is a factor that depends on the details of the disk-magnetosphere interaction and ranges between 0.5 and 1 (see, e.g., Bozzo et al. 2009 for a discussion of the various models; Campana et al. 2018 recently determined $\xi = 0.5$ by using data from different classes of accreting magnetic stars

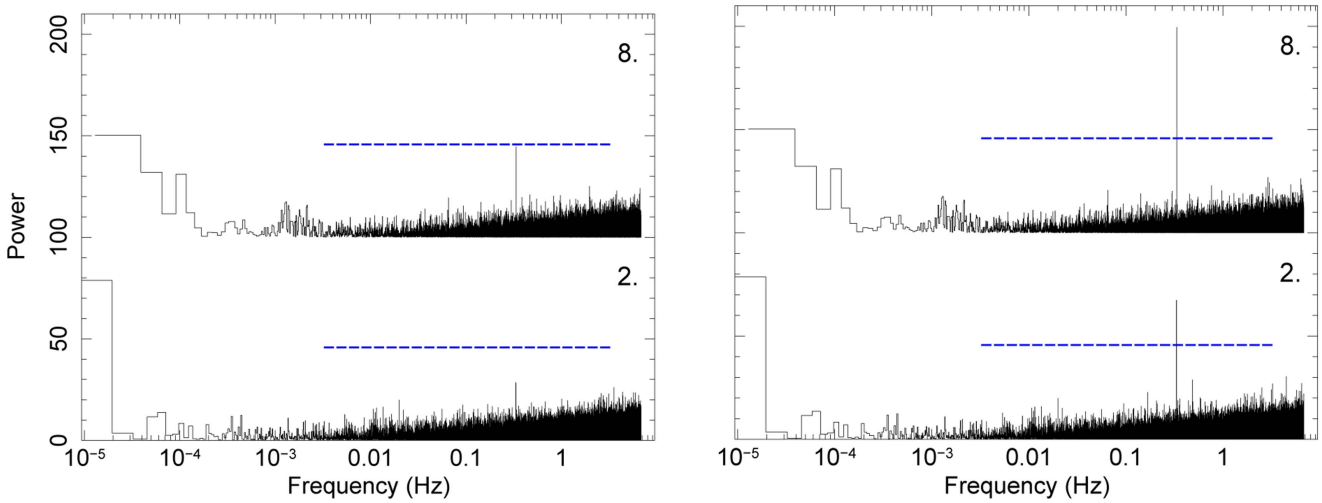

Figure 1. Left panel: power spectral density (PSD) of the pn 0.2–12 keV original light curves of two out of the nine data sets in which pulsations were detected (the labels identify the observations as in Table 1; the upper PSDs were shifted upward by 100 for displaying purposes). The blue dashed lines indicate the 3.5σ detection threshold, which takes into account the number of Fourier frequencies in the PSD. Right panel: same as before, but after correcting the photon arrival times of the two data sets for the orbital parameters derived from the phase fitting of Obs. #9 ($P_{\rm orb}$ and $a_{\rm X}$ sin i) and from the orbital correction pipeline (local $T_{\rm node}$; see Section 2 for details).

undergoing transitions to the propeller regime). The disk must be truncated at a radius larger than the NS radius, R_*, and smaller than the co-rotation radius ($R_{\rm co} = 3485\, M_{*,1.4}^{1/3}$ km, for a 3 s pulsar) for accretion-powered X-ray pulsations to be produced. The former limit originates from the requirement that the NS magnetosphere is not buried under the NS surface, and the latter implies that the NS rotation does not inhibit accretion through the propeller effect. Inserting the observed X-ray luminosity range ($L_{38} = 0.5$–2) in Equation (1), the condition $R_* < R_{\rm in} < R_{\rm co}$ is satisfied for $\mu_{28} = 0.05$–700. The observation of X-ray pulsations then binds the magnetic field strength at the poles of the NS to a broad range of $B_{\rm p} = 2\mu R_*^{-3} = 10^9$–$1.4 \times 10^{13}$ G, where the largest values correspond to a disk truncated at the co-rotation radius.

The torque applied by the disk onto the NS is expressed by $N = -2\pi I\dot{P}/P^2 = \dot{M}\sqrt{GM_*R_{\rm in}}\,F(\omega)$, where I is the NS moment of inertia, $\omega = (R_{\rm in}/R_{\rm co})^{3/2}$ is the fastness parameter, and the function $F(\omega)$ describes the reversal of the torque when the inner disk radius approaches the co-rotation radius (Ghosh & Lamb 1979). Assuming that 3X J0042 is a *slow rotator* spinning far from equilibrium and thus that the disk is truncated well inside the co-rotation radius (i.e., $\omega \ll 1$ and $F(\omega) = 1$), and using Equation (1) to express the inner disk radius, we get

$$\dot{P}_{-11} = -2.75\, I_{45}^{-1}(\eta^{-1}L_{38})^{6/7}\xi_{0.5}^{1/2}\, M_{*,1.4}^{-3/7}\, R_{*,10}^{6/7}\, \mu_{28}^{2/7} \qquad (2)$$

for a $P = 3$ s pulsar. Here, $\dot{P}_{-11}$ is the spin-up rate in units of 10^{-11} and I_{45} is the NS moment of inertia in units of 10^{45} g cm^{-2}. Considering an average luminosity of $L_{38} \simeq 2$, the average spin-up rate observed from 3X J0042, $\dot{P}_{-11} \sim -6$, is explained if the pulsar has a dipole magnetic moment of $\mu_{28} \simeq 1.9\, I_{45}^{7/2}\, M_{*,1.4}^{3/2}\, R_{*,10}^{-3}\, \eta^{-3}\, \xi_{0.5}^{-7/4}$. Considering the range of values that can be taken by $\xi = 0.5$–1, this corresponds to a magnetic field at the NS poles of $B_{\rm p} \simeq$ (1–4) $\times 10^{10}$ G. The spin-down rate of 3X J0042 was observed to increase from $\dot{P}_{-11} \sim -4.2$ to -8.5 while the X-ray luminosity increased from $L_{38} = 0.9$ to 2.0, suggesting a relation $P \propto L_{\rm X}^{\alpha}$ with $\alpha \simeq 1$. This value is close to that predicted by simple models of the disk-magnetosphere interaction ($\alpha = 6/7$) when the pulsar is a *slow rotator*, lending support to the above interpretation. However, the spin-up timescale $P/\dot{P} \simeq 1600$ year is very short compared to the typical duration of the spin-up accretion phase of pulsars in LMXBs, 10^8–10^9 year (e.g., Tauris et al. 2012), casting doubts on this interpretation. On the other hand, there are known cases of X-ray pulsars accreting close to or above the Eddington luminosity with much shorter spin-up timescales than expected (e.g., some ultraluminous X-ray pulsars; Israel et al. 2017). In this scenario a related object to 3X J0042 might be IGR J17480–2446, a 90 ms transient X-ray pulsar in a LMXB with a companion with mass $>0.4\, M_{\odot}$, which belongs to the globular cluster Terzan 5 (Papitto et al. 2011) and an inferred magnetic field in the (0.5–1.5) $\times 10^{10}$ G range (Papitto et al. 2012, see also Cavecchi et al. 2011).

Alternatively, the pulsar might be spinning close to the equilibrium value (i.e., $R_{\rm in} \simeq R_{\rm co}$). The magnetic field required in this case would be $B_{\rm eq} = 1.9 \times 10^{13}\, R_{*,10}^{-5/2}\, M_{*,1.4}^{1/3}\, \xi_{0.5}^{-7/4}(\eta^{-1}L_{38})^{1/2}$ G, i.e., much larger than that of the previous scenario. The expected spin-up torque depends crucially on the shape of the function $F(\omega)$. Taking $F(\omega) = 1 - \omega^2$ (Ertan et al. 2009), the observed average spin-up rate is reproduced with $\omega = 0.92$ (i.e., $R_{\rm in} = 0.\,95R_{\rm co}$). If 3X J0042 is spinning close to equilibrium, it is expected that small variations of the mass accretion rate might induce large variations of the spin-up rate or even torque reversals (see Camero-Arranz et al. 2010 for the case of 4U 1626–67). In this scenario, the spin-up timescale would not necessarily be related to the time elapsed because the onset of accretion and the hard X-ray spectral component of 3X J0042 extending up to tens of keV might be more easily interpreted.

Our results demonstrate that 3X J0042 is a 3 s X-ray pulsar accreting close to the Eddington rate from a low-mass companion. The evolution of the spin period, together with the other source properties, indicates that the pulsar might be either in the slow rotator regime and possess a magnetic field of $\sim 10^{10.5}$ G, or be a a quasi-equilibrium rotator with a field of

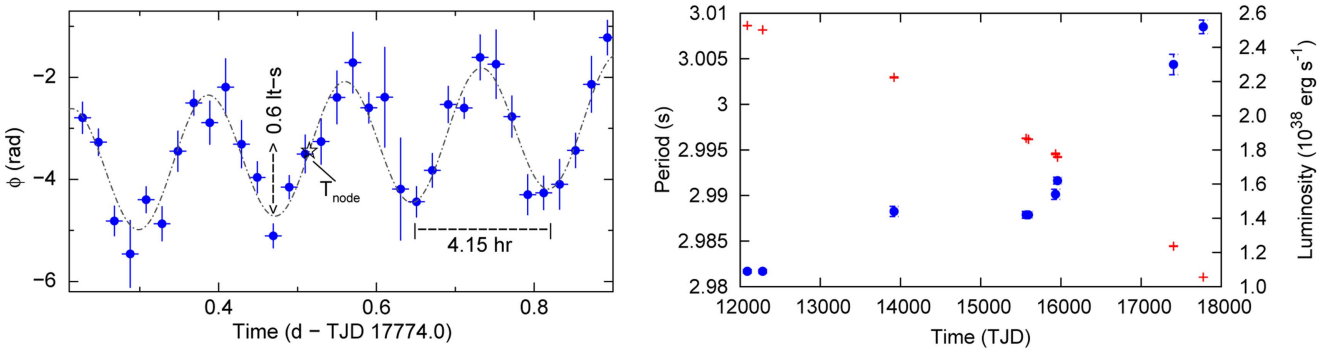

Figure 2. Left panel: pulse phases as a function of time for the longest *XMM-Newton* observation of 3X J0042 (Obs. #9). The Doppler orbital modulation is evident and the main orbital parameters measured (P_{orb}, $a_X \sin i$, and T_{node}) are indicated graphically. Right panel: the period (red crosses) and 0.2–12 keV luminosity evolution (blue dots). The spin-up rate increase occurring approximately after TJD 16000 appears to correlate with the luminosity rise.

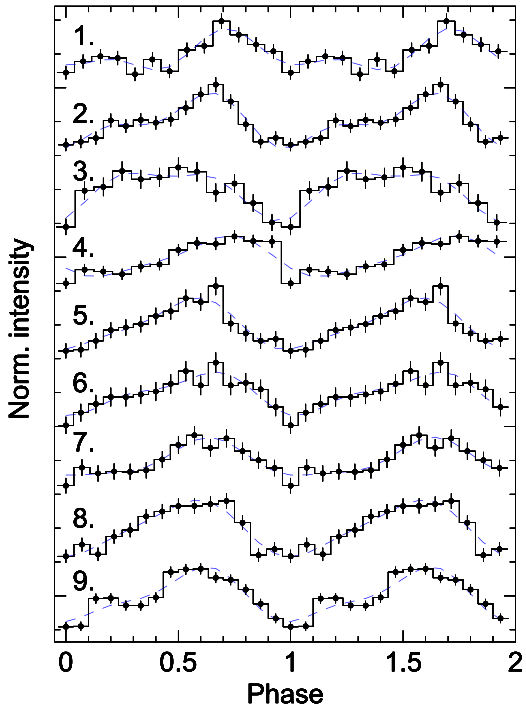

Figure 3. *XMM-Newton*/pn orbit-corrected 0.2–12 keV light curves folded at the period measured in each data set where the ∼3 s signal was detected. Two cycles are shown for clarity, and the curves have been aligned in phase and shifted vertically in an arbitrary fashion for display purposes.

$\sim 10^{13}$ G. In the latter interpretation, a transition to the propeller regime and thus a drastic reduction of the source luminosity would ensue in response to a decrease of the disk mass inflow rate. Therefore, the detection of a transient behavior from 3X J0042 would provide decisive support in favor of the quasi-equilibrium rotator interpretation.

This research is based on observations obtained with *XMM-Newton*, an ESA science mission with instruments and contributions directly funded by ESA Member States and NASA. This research was supported by high-performance computing resources awarded by CINECA (MARCONI), under the ISCRA initiative to the "PASTA-X project," and also through the INAF–CHIPP high-performance computing project resources and support. P.E. acknowledges funding in the framework of the NWO Vidi award A.2320.0076. L.S., A.P., and G.L.I. acknowledge financial contribution from ASI-INAF agreement I/037/12/0. A.P. also acknowledges funding from the EU Horizon 2020 Framework Programme for Research and Innovation under the Marie Skłodowska-Curie Individual Fellowship grant agreement 660657-TMSP-H2020-MSCA-IF-2014.

Facility: XMM-Newton (EPIC).

Software: FTOOLS (v6.21; Blackburn 1995), SAS (v16; Gabriel et al. 2004).

ORCID iDs

Guillermo A. Rodríguez Castillo https://orcid.org/0000-0003-3952-7291
Gian Luca Israel https://orcid.org/0000-0001-5480-6438
Paolo Esposito https://orcid.org/0000-0003-4849-5092
Alessandro Papitto https://orcid.org/0000-0001-6289-7413
Luigi Stella https://orcid.org/0000-0002-0018-1687
Andrea Tiengo https://orcid.org/0000-0002-6038-1090
Martino Marelli https://orcid.org/0000-0002-8017-0338

References

Baumgartner, W. H., Tueller, J., Markwardt, C. B., et al. 2013, ApJS, 207, 19
Blackburn, J. K. 1995, in ASP Conf. Ser. 77, Astronomical Data Analysis Software and Systems IV, ed. R. A. Shaw, H. E. Payne, & J. J. E. Hayes (San Francisco, CA: ASP), 367
Bozzo, E., Stella, L., Vietri, M., & Ghosh, P. 2009, A&A, 493, 809
Camero-Arranz, A., Finger, M. H., Ikhsanov, N. R., Wilson-Hodge, C. A., & Beklen, E. 2010, ApJ, 708, 1500
Campana, S., Stella, L., Mereghetti, S., & de Martino, D. 2018, A&A, 610, A46
Cavecchi, Y., Patruno, A., Haskell, B., et al. 2011, ApJL, 740, L8
Dall'Osso, S., Israel, G. L., Stella, L., Possenti, A., & Perozzi, E. 2003, ApJ, 599, 485
De Luca, A., Salvaterra, R., Tiengo, A., et al. 2016, in Astrophysics and Space Science Proc. 42, The Universe of Digital Sky Surveys, ed. N. Napolitano et al. (Cham: Springer International Publishing), 291
Ertan, Ü., Ekşi, K. Y., Erkut, M. H., & Alpar, M. A. 2009, ApJ, 702, 1309
Esposito, P., Israel, G. L., Belfiore, A., et al. 2016, MNRAS, 457, L5
Frank, J., King, A. R., & Lasota, J.-P. 1987, A&A, 178, 137
Gabriel, C., Denby, M., Fyfe, D. J., et al. 2004, in ASP Conf. Ser. 314, Astronomical Data Analysis Software and Systems (ADASS) XIII, ed. F. Ochsenbein, M. G. Allen, & D. Egret (San Francisco, CA: ASP), 759
Ghosh, P., & Lamb, F. K. 1979, ApJ, 234, 296
Holland, S. 1998, AJ, 115, 1916
Israel, G. L., Belfiore, A., Stella, L., et al. 2017, Sci, 355, 817
Israel, G. L., & Stella, L. 1996, ApJ, 468, 369
Marelli, M., Tiengo, A., de Luca, A., et al. 2017, ApJL, 851, L27
Papitto, A., D'Aì, A., Motta, S., et al. 2011, A&A, 526, L3

Papitto, A., di Salvo, T., Burderi, L., et al. 2012, MNRAS, 423, 1178
Revnivtsev, M. G., Sunyaev, R. A., Krivonos, R. A., Tsygankov, S. S., & Molkov, S. V. 2014, AstL, 40, 22
Strüder, L., Briel, U., Dennerl, K., et al. 2001, A&A, 365, L18
Tauris, T. M., Langer, N., & Kramer, M. 2012, MNRAS, 425, 1601
Turner, M. J. L., Abbey, A., Arnaud, M., et al. 2001, A&A, 365, L27
Vulic, N., Gallagher, S. C., & Barmby, P. 2016, MNRAS, 461, 3443
Yukita, M., Ptak, A., Hornschemeier, A. E., et al. 2017, ApJ, 838, 47
Yukita, M., Tzanavaris, P., Corbet, R., et al. 2018, in AAS Meeting 231 Abstracts, 33.301
Zolotukhin, I. Y., Bachetti, M., Sartore, N., Chilingarian, I. V., & Webb, N. A. 2017, ApJ, 839, 125